Terr. Atmos. Ocean. Sci., Vol. 19, No. 6, 729-741, December 2008 doi: 10.3319/TAO.2008.19.6.729(PT)

Seismic Tomography off SW Taiwan: A Joint Inversion from OBS and Onshore Data of 2006 Pingtung Aftershocks

Yen-Che Liao[1], Shu-Kun Hsu[1,*], Chien-Hsing Chang[2], Wen-Bin Doo[1], Mei-Yi Ho[2], Chung-Liang Lo[1], and Chao-Shing Lee[3]

[1] *Institute of Geophysics, National Central University, Chung-Li, Taiwan, ROC*
[2] *Seismology Center, Central Weather Bureau, Taipei, Taiwan, ROC*
[3] *Institute of Applied Geoscience, National Taiwan Ocean University, Keelung, Taiwan, ROC*

Received 29 February 2008, accepted 26 September 2008

ABSTRACT

On 26 December 2006, two M_L = 7.0 events occurred offshore south of Pingtung; one is associated with a normal-faulting and the other with a strike-slip faulting. The area where these earthquakes were located is not usually expected to have large earthquakes. We deployed 11 short period OBSs over the source zone for one week and recorded a series of aftershocks which were also recorded on land at the CWB network stations. The joint dataset made it possible for us to perform a 3-D velocity tomography and earthquake relocation in this region, where the velocity structures were not well known and location of earthquakes with only land data was uncertain.

The tomographic results show a prominent high Vp perturbation zone (HVPZ) that we consider as the uppermost mantle of the subducted plate dipping from SW to NE beneath southern Taiwan. Most of the relocated earthquakes are distributed just above the HVPZ or near and along the bottom of a relatively low velocity subducted crust. Our results show that the subducted and bent Eurasian plate off SW Taiwan could have been unbent and become an upwards concave geometry for the upper 30 km. The main shock is near the bottom of the inflected surface. The distribution of the earthquake sequence generally displays in a NW-SE direction, coinciding with the plate convergence orientation between the Philippine Sea Plate and Eurasian Plate. This orientation also follows a relatively low Bouguer gravity anomaly stripe that is due to a heavy loading of the Taiwan orogen on the east-dipping Eurasian Plate. Considering that the hypocenter of the first main-shock is near the bottom of the aftershocks, we suggest that the first normal faulting earthquake was caused by an unbending effect in the subducting crust and this event triggered the release of accumulated energy between the Philippine Sea Plate and Eurasian Plate. Thus, we suggest that the rupture surface of the Pingtung earthquake sequence had propagated upwards and northwestward in the direction of plate convergence.

Key words: Slab bending, Pingtung earthquake, Tectonics, Tomography, Taiwan

Citation: Liao, Y. C., S. K. Hsu, C. H. Chang, W. B. Doo, M. Y. Ho, C. L. Lo, and C. S. Lee, 2008: Seismic tomography off SW Taiwan: A joint inversion from OBS and onshore data of 2006 Pingtung aftershocks. Terr. Atmos. Ocean. Sci., 19, 729-741, doi: 10.3319/TAO.2008.19.6.729(PT)

1. INTRODUCTION

The Philippine Sea Plate is moving northwestward at a speed of ca. 8 cm yr^{-1} relative to the Eurasian Plate (Seno et al. 1993; Yu et al. 1997). In the east of Taiwan, the Philippine Sea Plate has subducted northward beneath the Eurasian Plate (Fig. 1a). In southern Taiwan, the Eurasian Plate has subducted along the Manila Trench beneath the Philippine Sea Plate. The geometry of the east-dipping Eurasian slab can be imaged beneath southern Taiwan from tele-seismic tomography (Wang et al. 2006). Taiwan Island has been created due to the oblique convergence of the interlaced Eurasian and Philippine Sea plates (Sibuet and Hsu 2004). The active convergence has generated enormous earthquakes, mainly distributed in middle-western Taiwan and along the Luzon-Ryukyu arc system (Wang and Shin 1998; Lo and Hsu 2005). The intensive mountain building has generated loading on the east-dipping Eurasian Plate and has simultaneously developed a foreland basin system in the west of the Taiwan mountain belt to receive sediments (Yu and Chou 2001; Lin and Watts 2002). The eastward dipping

* *Corresponding author*
E-mail: hsu@ncu.edu.tw

flexure of the Eurasian Plate is reflected by a relatively low Bouguer gravity anomaly around the western Taiwan (Hsu et al. 1998) (Fig. 1).

Due to the incipient collision in southern Taiwan, the continuation of the Manila Trench to the north of 21.5°N and thus the seismic potential of this structure are often questioned. Basically, the region is considered as a transition zone between the Eurasian continental crust and the South China Sea oceanic crust (Hsu et al. 2004; Tsai et al. 2004; Yeh and Hsu 2004; McIntosh et al. 2005); the crust is about 12 km thick. The M_L = 7.0 Pingtung earthquake occurred at 1226 UTC 26 Dec. 2006 to the west and southwest of the Hengchun peninsula was not anticipated; eight minutes later, another M_L = 7.0 earthquake occurred to the northwest of the first one. These large earthquakes had surprised geoscientists and aroused controversy on the tectonic context of the main shock and aftershocks.

With large number of earthquakes in and around Taiwan, the seismic velocity structures beneath Taiwan Island and the western part of Ryukyu trench have been relatively well imaged through regional earthquake tomography (e.g., Hsu 2001; Kim et al. 2005; Lin et al. 2007; Wu et al. 2007). In contrast, the offshore area of SW Taiwan with the exception of some crustal-scale seismic profiles (Nakamura et al. 1998; McIntosh et al. 2005) is still poorly understood; the absence of ocean-bottom seismic stations poses a severe limitation on local tomographic studies. Since we expected that a great number of aftershocks would follow the main Pingtung earthquakes, we deployed eleven OBSs in the source area off SW Taiwan to record them. The resulting increase in seismic ray coverage provides better resolution for tomographic inversion. By combining the arrival times of

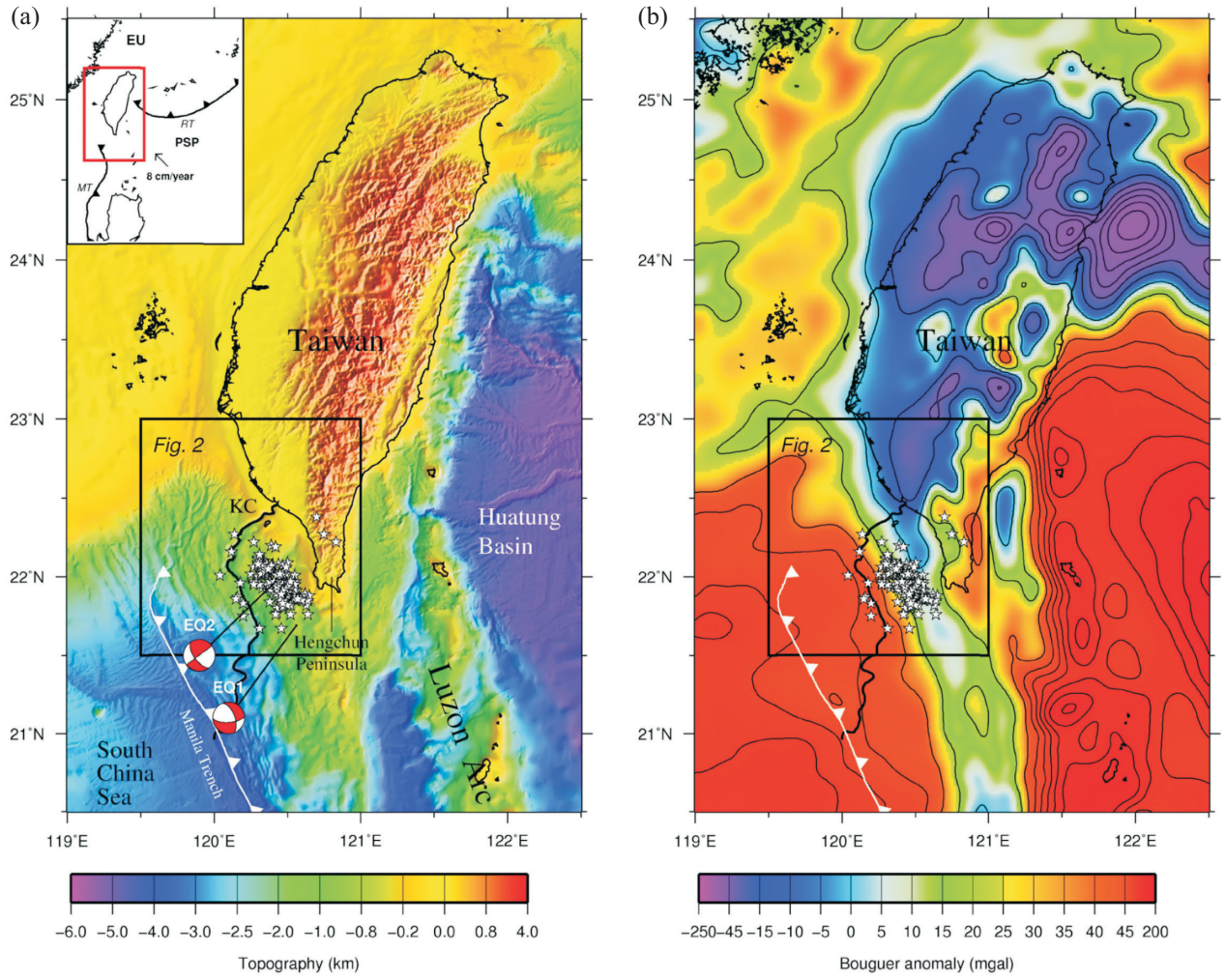

Fig. 1. (a) Topography of the Taiwan region. The inset shows the tectonic framework of the region. White stars indicate the epicenters of the aftershocks recorded by Central Weather Bureau within 46 hours after the main shocks on 26 December 2006. Focal mechanisms of the major earthquakes are from the results of Chen et al. (2007). The Kaoping Canyon (KC) is traced by a heavy line. EU: Eurasian Plate; PSP: Philippine Sea Plate; MT: Manila Trench; RT: Ryukyu Trench. (b) Bouguer anomaly of the Taiwan region. Symbols have the same meanings as in (a). Note that the earthquakes trending mainly NW-SE is located along the slope of a relatively low Bouguer anomaly stripe.

the aftershocks from our OBS data with those from CWBSN land stations, we perform a 3-D Vp tomography for the offshore region of SW Taiwan to investigate the relationship between the tectonic structure and the earthquake mechanism off SW Taiwan.

2. SEISMIC TOMOGRAPHY

2.1 Data and Methodology

Eleven OBSs were deployed in the offshore area of southwest Taiwan (Fig. 2) for about one week after the Pingtung earthquake, from 1700 UTC 27 Dec. 2006 to 2300 UTC 3 Jan. 2007. The OBS sensor is Geo Space GS-11D with a natural frequency of 4.5 Hz. The acquisition system is based on a 4-channel 24 bits CS5372/76 analog to digital convertor together with input signal amplification. The sampling rate of our data was set as 125 Hz with timing provided by GPS clock. The time drift was corrected by using a liner interpolation. We have picked all the arrival time from OBS waveforms manually without prior information of CWB catalog. An example to show the quality of the seismograms was represented in Fig. 3.

Since our interest lies not only in the source area of the Pingtung earthquake but also its surrounding, we combine arrival times from both OBSs with those from CWBSN land stations. In total, there are 21 CWBSN stations for 414 events with 3669 P arrival times; and 11 OBS stations for 454 events with 4234 P arrival times that are used as our initial input (Fig. 4). We first re-determine the origin times and locations of the earthquakes and calculated the residual times by the layer model shown in Table 1. We chose a subset of events based on (1) the magnitude of events greater than two, (2) events recorded by more than four stations, and (3) the travel-time residuals are less than 2 sec after the relocation.

The tomography inversion program SIMUL2000 (Thurber and Eberhart-Phillips 1999) was used for our 3-D Vp inversion. On the basis of checkerboard resolution tests, a grid spacing of 8 km is adopted except at northern and southern ends of our model where 15 km spacing is used. The locations of 15 × 17 grid points are shown in Fig. 4. In the vertical grids are located at the depths of -2, 1, 3, 6, 9, 13, 18, 23, 28, 35, 42, 50, 70, and 130 km. We use an initial 1-D layered model constructed on the basis of the OBS refraction results of McIntosh et al. (2005, Table 1). For the velocity inversion, the velocity grids were established as 3-D grid points with linear gradients. An appropriate damping value is adopted after inspecting the trade-off curve be-

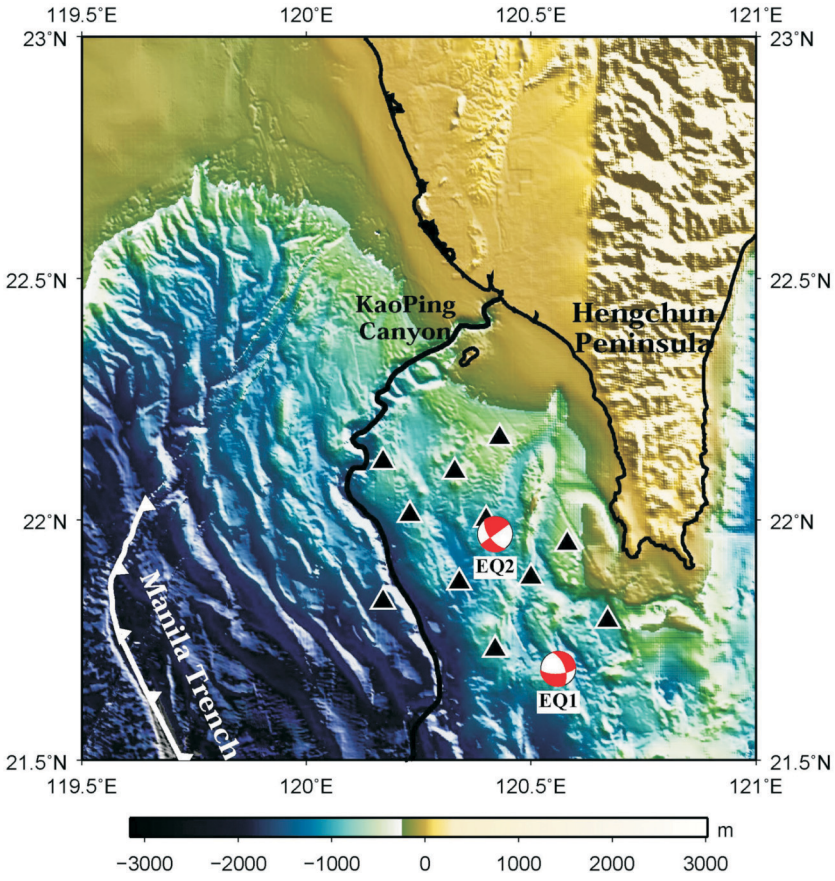

Fig. 2. Bathymetry off SW Taiwan. Eleven OBS locations were labeled by black triangles.

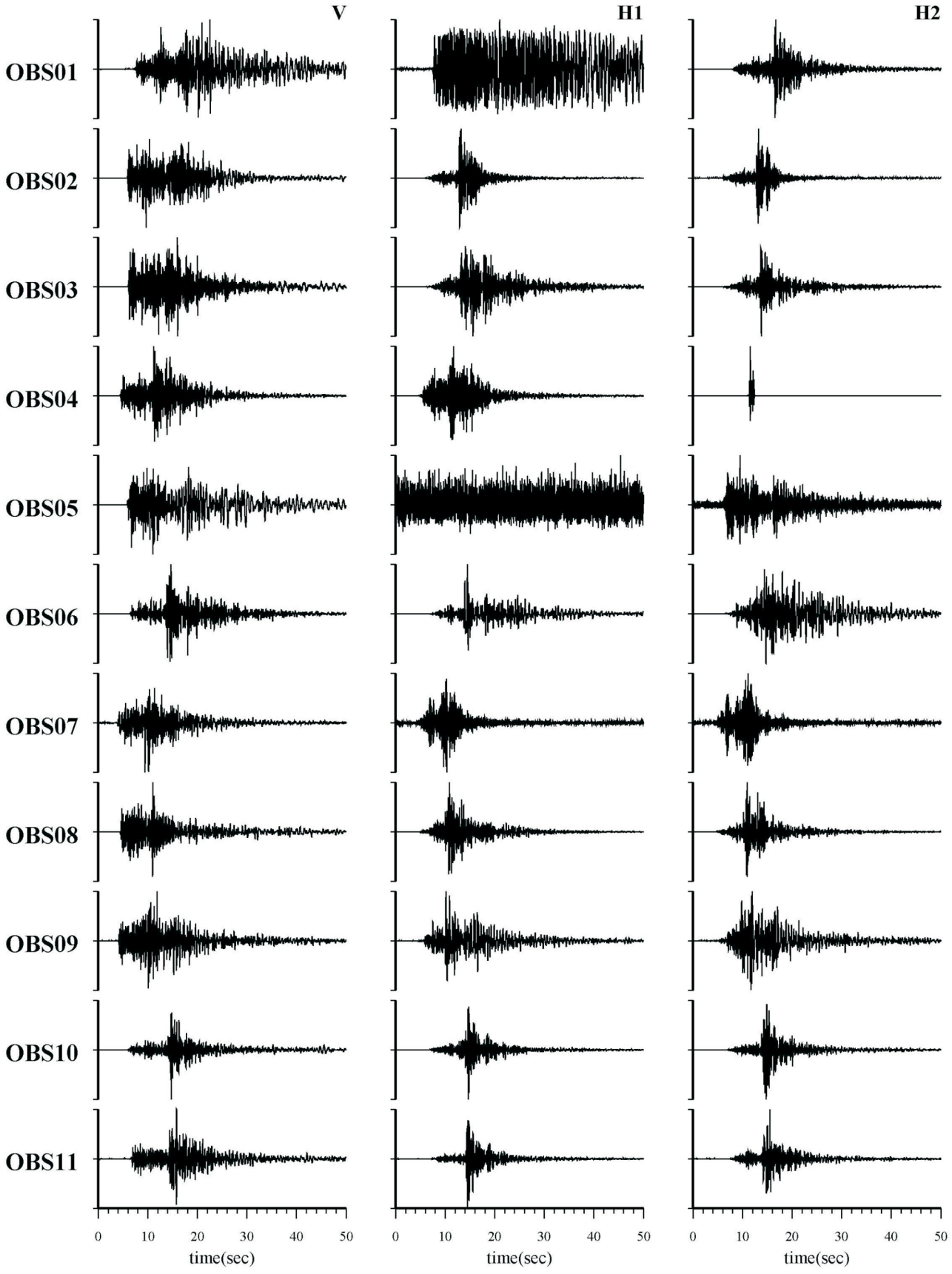

Fig. 3. An example shows the quality of the seismograms. V means the vertical component; H1 and H2 mean two horizon components. The amplitudes are normalized to the maximum amplitude, individually.

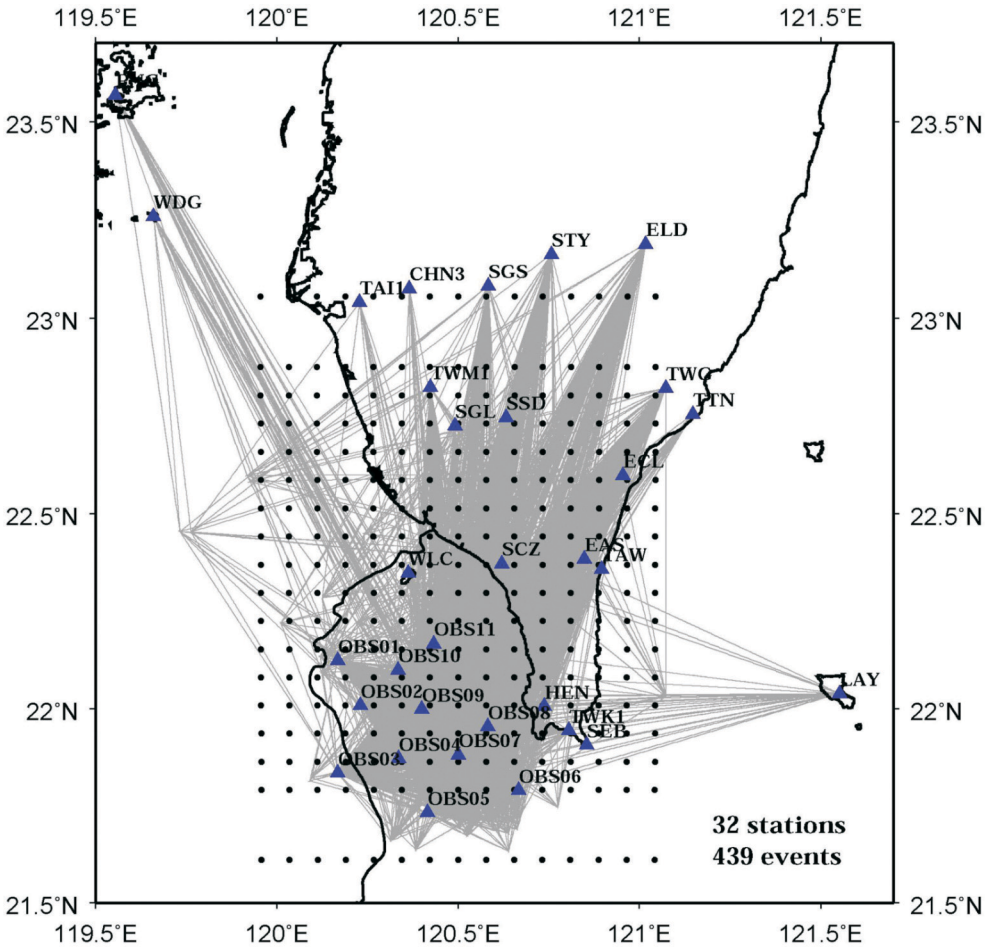

Fig. 4. The coverage of seismic rays (gray lines) between the stations and the epicenters. The observed stations used in this study are marked by blue triangles.

Table 1. Initial Vp layer model.

Grid Number	Depth (km)	Vp (km s^{-1})
1	-2	1.50
2	1	1.82
3	3	2.84
4	6	3.07
5	9	3.80
6	13	5.33
7	18	7.11
8	23	7.36
9	28	7.63
10	35	7.92
11	42	8.02
12	50	8.05
13	70	8.16
14	130	8.35

tween the data variance and the model variance (Eberhart-Phillips 1986). We use a damping value of 100 in the tomographic inversion.

2.2 Resolution Test and Flexible Gridding

In order to investigate the optimum spatial resolution from the existing ray coverage, the checkerboard resolution test (CRT) (Humphreys and Clayton 1988; Zhao et al. 1992) was applied. In practice, ±6% of velocity perturbations was assigned alternately to the grids to make up the checkerboard model and generated the synthetic traveltimes. Secondly, the unperturbed layer model was used as the initial model; meanwhile, the synthetic traveltimes from the perturbed model were used as input to invert the checkerboard velocity model. The recovery of checkerboard pattern at depths shallower than 9 km is poor (Fig. 5), apparently due to the lack of ray coverage. The better recovery pattern is located between Kaoping canyon and Hengchun peninsula at depths between 18 and 35 km (Fig. 5). In the region with poor recovery, we adopted the linear flexible gridding technique

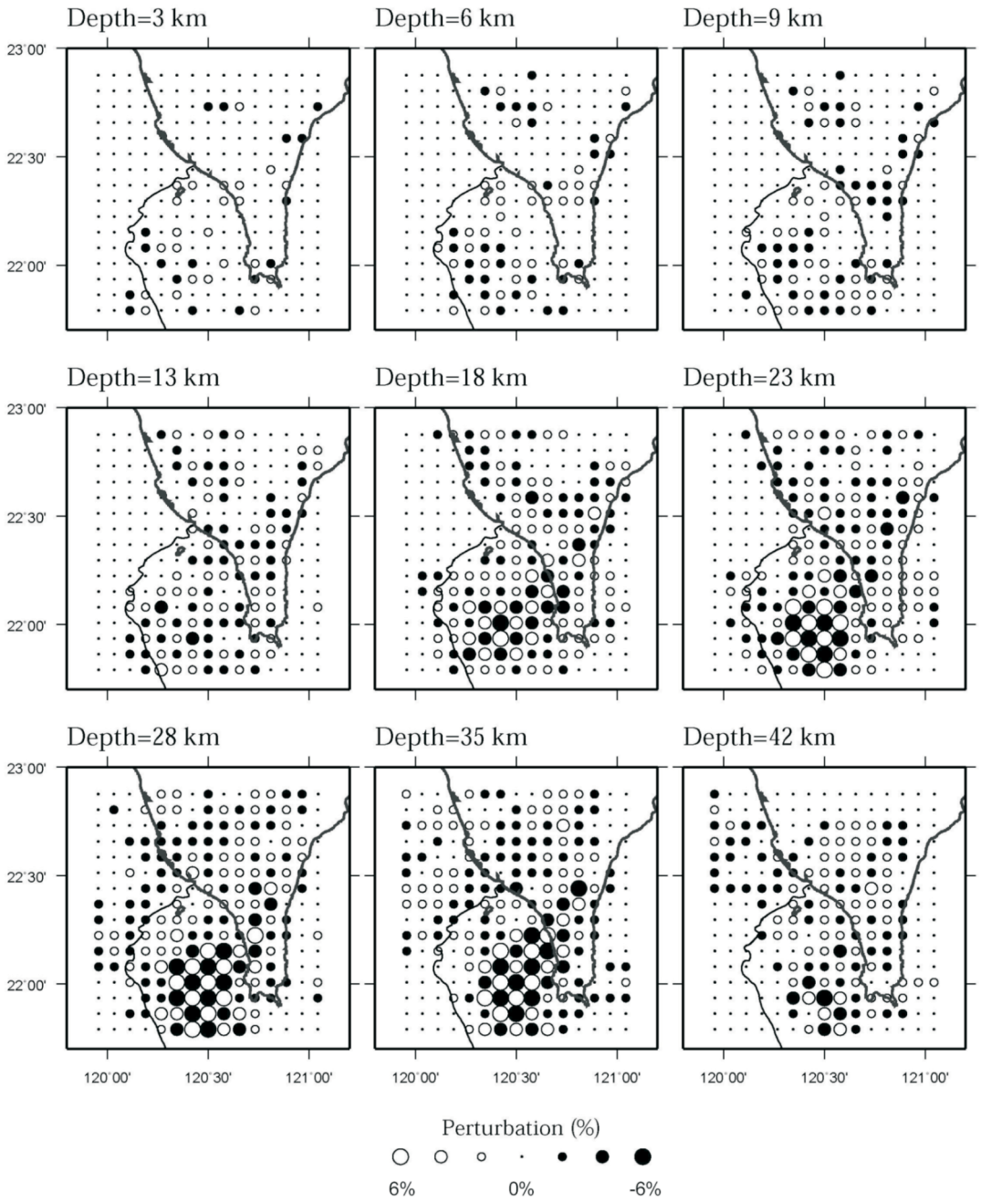

Fig. 5. The results of checkerboard test in individual vertical grid plane from 3 to 42 km.

suggested by Thurber and Eberhart-Phillips (1999); we designate slave grids with master grids and then do the inversion processing (Fig. 6). The values of designated slave grids depend only on the values of the master grids during the inversions. During the computation, F-test was used to provide a stopping criterion. Finally, 439 events of earthquake with 6295 travel-time readings were employed in 7 iterations in our inversion.

To access the reliability of our results, the diagonal value of resolution is contoured in interval 0.1 and displayed in Fig. 7. The regions with better resolution coincide with those shown in the checkerboard test (Fig. 5). However, the resolutions are low and scattered toward the land.

3. RESULTS AND DISCUSSIONS

As demonstrated by previous tests, we will mainly focus our discussions in the region where is a more reliable velocity structure from our P wave tomography.

First, a prominent feature in the inverted velocity struc-

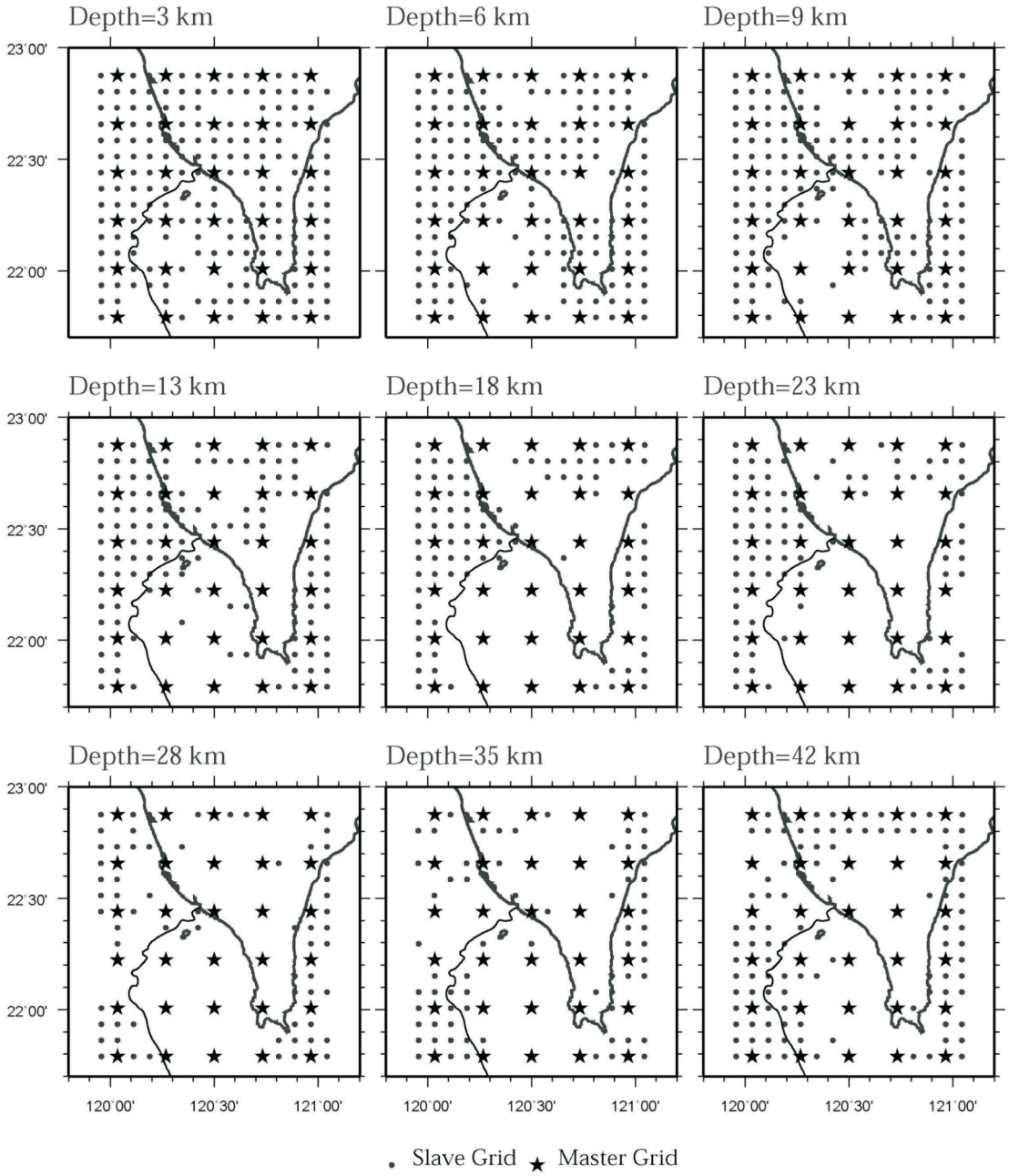

Fig. 6. Linear flexible grid settings are established to compensate the poor checkerboard recovery. Black stars and dots are master and linked slave grids, respectively.

tures is a NW-SE trending high velocity structure at depth of 18 and 23 km (Fig. 8). This relatively high velocity zone (HVPZ) generally exists to the east of the middle reach of the Kaoping Canyon, particularly from depth 10 to 30 km (the blue area in Figs. 9 and 10). The NW-SE trending feature is consistent with a low Bouguer anomaly strip off SW Taiwan (Hsu et al. 1998). Based on the interpretation of Bouguer anomalies of Hsu et al. (1998), the subducting South China Sea plate bends along the NW-SE trend. The velocity profile AA', close to the second main-shock, is roughly perpendicular to the middle reach of the Kaoping Canyon (Fig. 9). In profile AA', the HVPZ deepens from SW to NE and is considered as the uppermost mantle of the subducted plate. Above the HVPZ, a low velocity zone lies above the HVPZ, and it could be considered as the subducted crust (Fig. 9). The earthquake hypocenters are generally distributed above HVPZ and near the bottom of the subducted crust (Fig. 10). As shown in Fig. 10, the first main shock of the Pingtung earthquakes is situated near the bottom of the earthquake cluster. Compared to the Pingtung

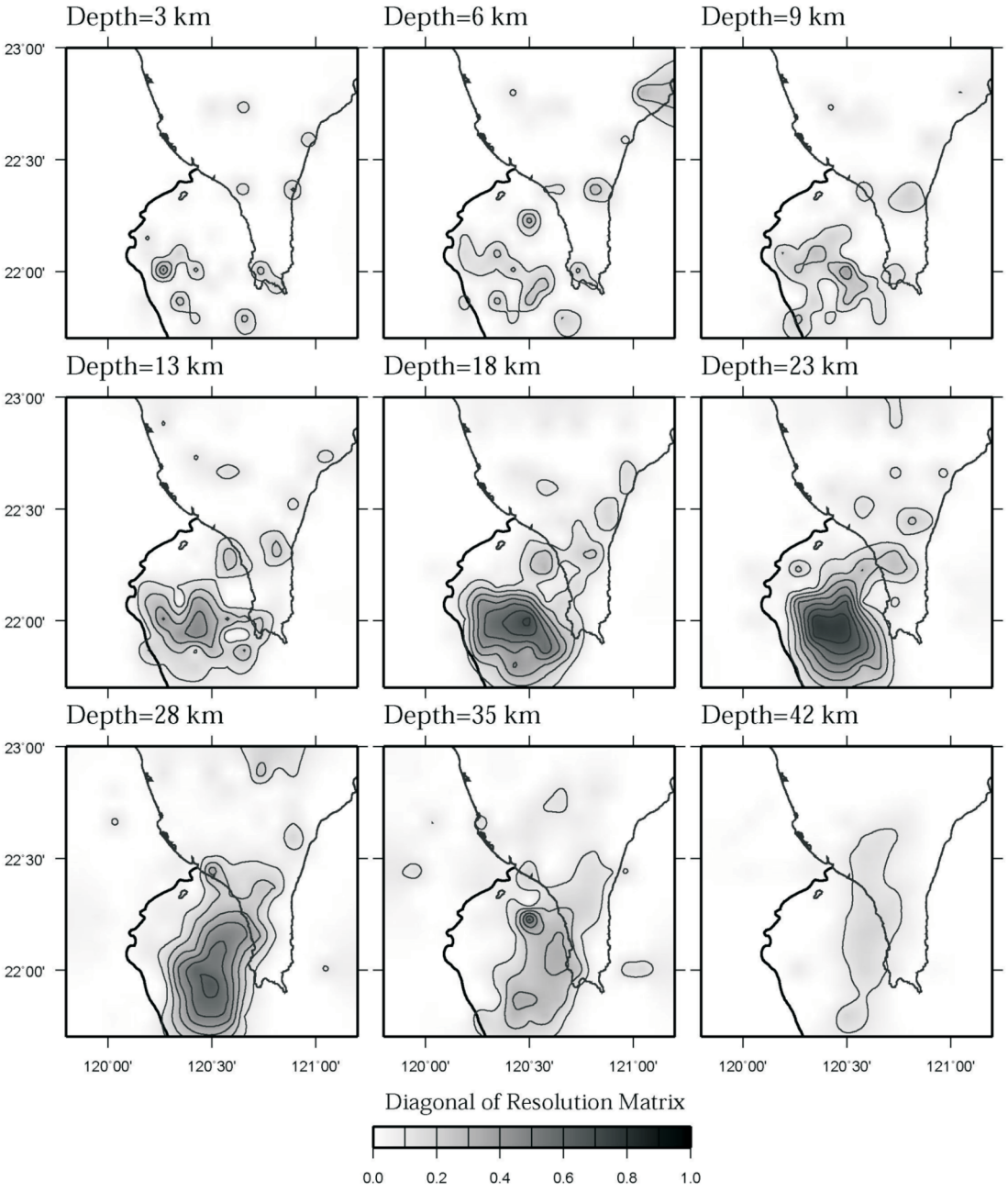

Fig. 7. The results of diagonal values of resolution matrix. The contour interval is 0.1.

aftershocks, it seems that the main shock triggered the earthquake sequence and the earthquake rupture has propagated upwards and northwards in the direction of plate convergence (Fig. 10).

Comparing the distribution of the aftershocks with the Bouguer anomaly, it is noticed that most of the aftershocks epicenters are distributed near the slope of a low Bouguer anomaly zone (Fig. 1b). Accordingly, one may ascribe the mechanism of the main Pingtung earthquake off southwest Taiwan to the bending and faulting of the subducting Eurasian slab, and hence the shallow crustal earthquakes could be expected. Nevertheless, the earthquakes in this series are relatively deep, to about 30 km.

On the other hand, compared to the background seismicity, the relocated events of Pingtung aftershocks are placed amid the historic hypocenters (Fig. 11), although the hypocenters of Pingtung earthquakes are generally shallower. Profile BB' in Fig. 11 is in the same line of Profile AA' in Fig. 9 but it extends further to the NE. As shown in Fig. 11, the aftershocks follow the trend of the subduction earthquakes (mostly between the two dashed lines in Fig. 11). In general, the deeper part of the subducted slab is concave

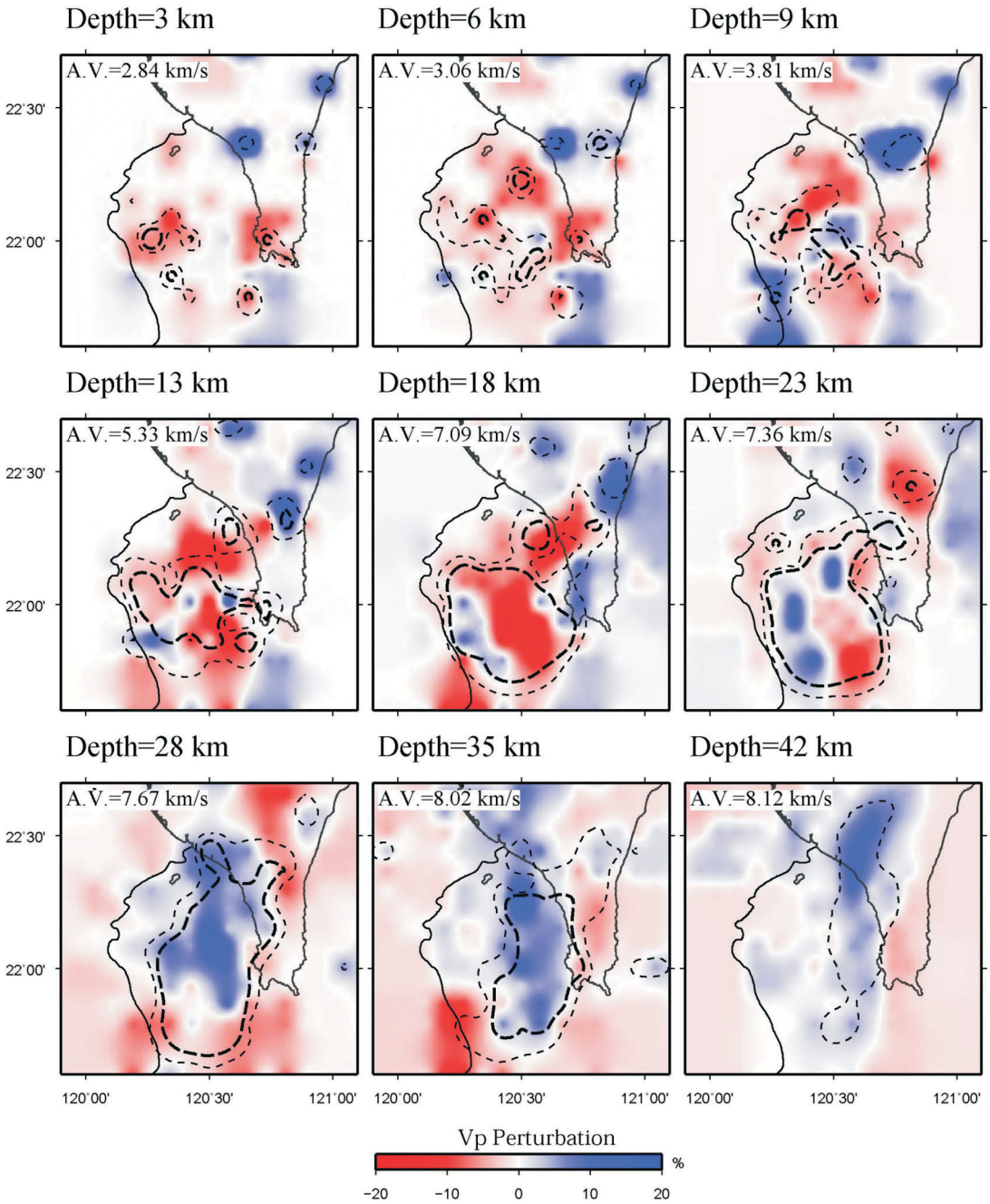

Fig. 8. The calculated P-wave velocity perturbation tomography. The average velocity (A.V.) means the average value of the velocities of the same layer. Thick and thin dash-line contours represent the diagonal element of resolution matrix 0.2 and 0.1, respectively.

downwards except in the section where the Pingtung earthquake are located; here the subducted slab is concave upwards (Fig. 11). We propose that the bend of the subducted plate at depths around 30 km deep could have been caused by the stress generated in the unbending of lithosphere in the offshore area of SW Taiwan. If we consider that the earthquakes happened generally inside the subducted crust, the lower dash line in Fig. 11 may correspond to the Moho interface. The place where the main Pingtung earthquake occurred near the crust/upper mantle (Moho) boundary or near the bottom of the inflected crust is a good environment for incubating large earthquakes. A possible reason for the unbending phenomenon off SW Taiwan could be that the subducting crust is a transitional crust in the Eurasian continental margin and the overriding crust around the Hengchun Peninsula area has comparable denser crust as evidenced by the Bouguer anomaly shown in Fig. 1b.

The slab unbends to become sub-horizontal in our case

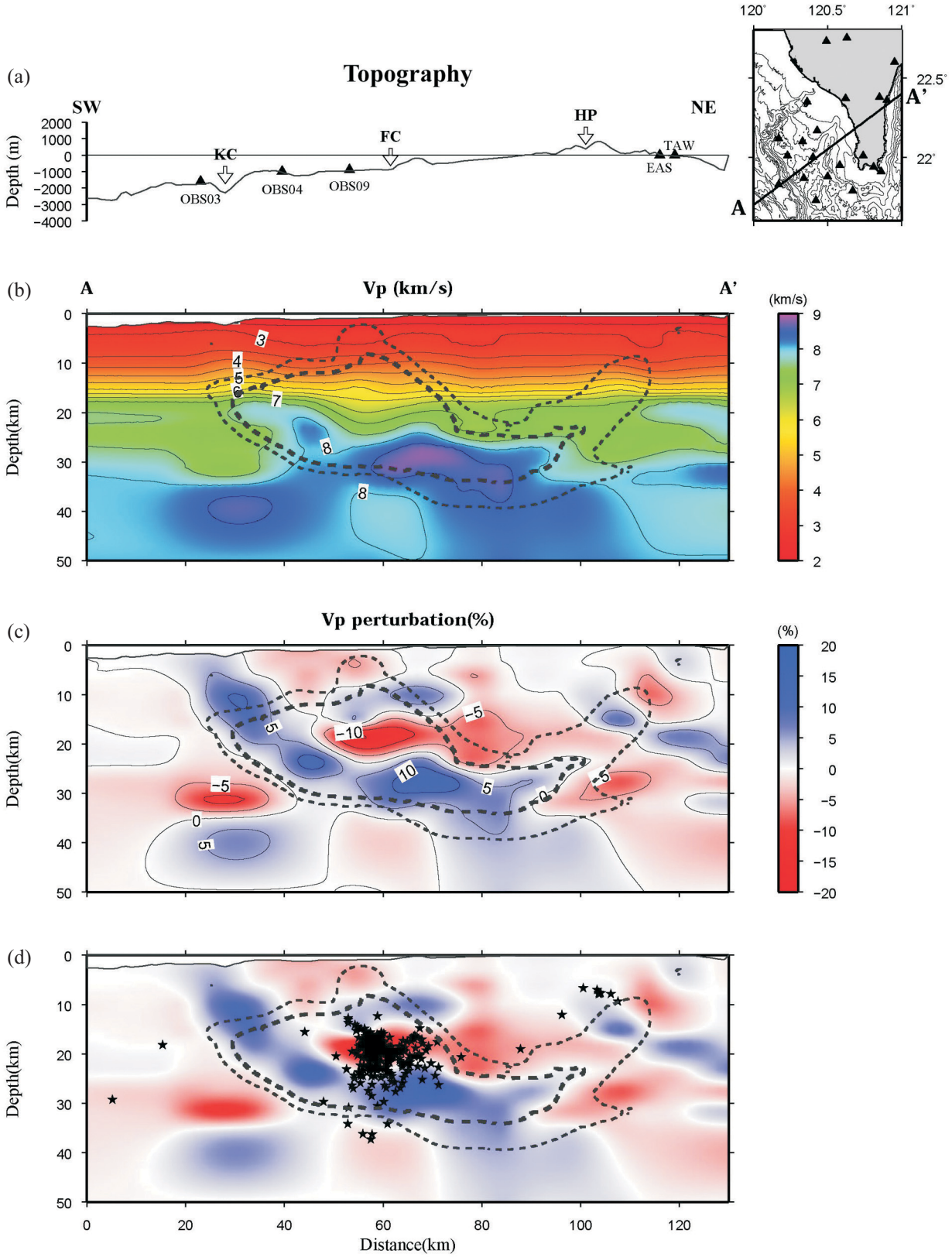

Fig. 9. Tomographic results along the profile AA'. (a) Topography along profile AA'. KC: Kaoping canyon; FC: Fangliao canyon; HP: Hengchun peninsula. (b) Vp tomography (c) Vp perturbation tomography (d) Locations of relocated events. The definition of the dash lines shown in this figure is the same as in Fig. 8.

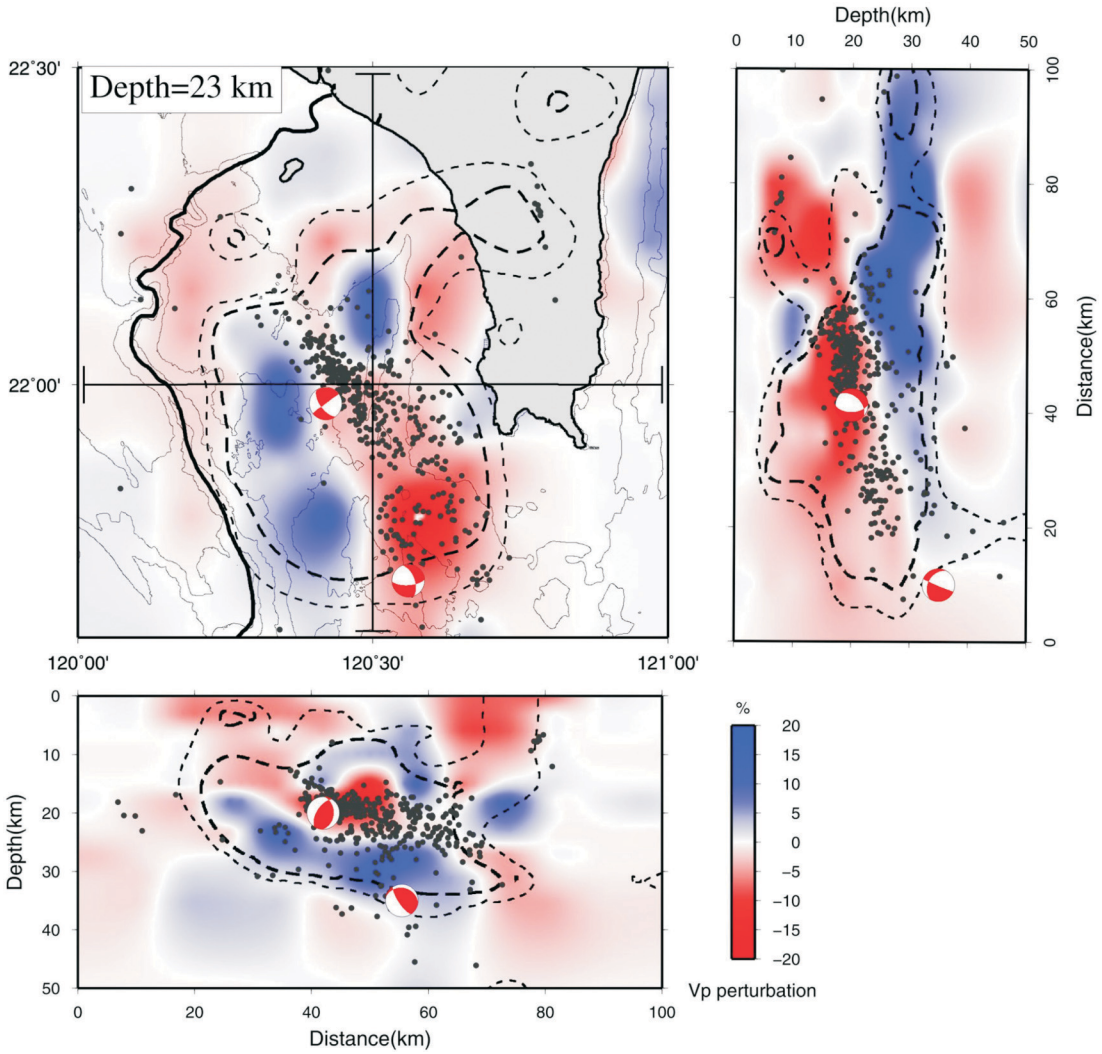

Fig. 10. Distribution of relocated events displayed on tomographic velocity perturbation at depth of 23 km. Vertical profiles along 22°N and 120.5°E are shown respectively. The definition of the dash lines shown in this figure is the same as in Fig. 8.

is similar to the case of the subduction zone of central Mexico (Gardi et al. 2000; Mikumo et al. 2002). Due to the bending stress from the flexural geometry of the subducted slab, large intraplate earthquakes with normal faulting may occur (Fig. 12).

4. CONCLUSIONS

We have used the travel-time data of Pingtung aftershocks from 11 OBSs and 21 CWBSN land stations to improve the seismic coverage off SW Taiwan. The joint data set allows a better inversion for a 3-D velocity model of that region. Our tomographic results show a relatively high Vp structure of the uppermost mantle and a relatively low Vp structure of the subducted crust. The geometry of the subducted slab off southern Taiwan is generally concave downwards except the section less than about 30 km where the subducted slab exhibits concave upwards. It suggests that the upper portion of the subducted slab off SW Taiwan has been unbent and may generate large intraplate normal faulting earthquakes. The Pingtung earthquakes were clustered near the bottom of the inflected crust. Compared the main shock with the aftershocks, we suggest that the Pingtung earthquake sequence have been initiated by the main normal faulting earthquake and then followed the NW-SE plate convergence direction to generate strike-slip faulting earthquakes. The rupture surface thus may have propagated upwards and northwestwards.

Acknowledgements We are indebted to Drs. Francis Wu and Andrew Lin for their helpful discussions. Careful reviews from Francis Wu and one anonymous reviewer have greatly improved the manuscript. This study was supported under a grant of the National Science Council, Taiwan.

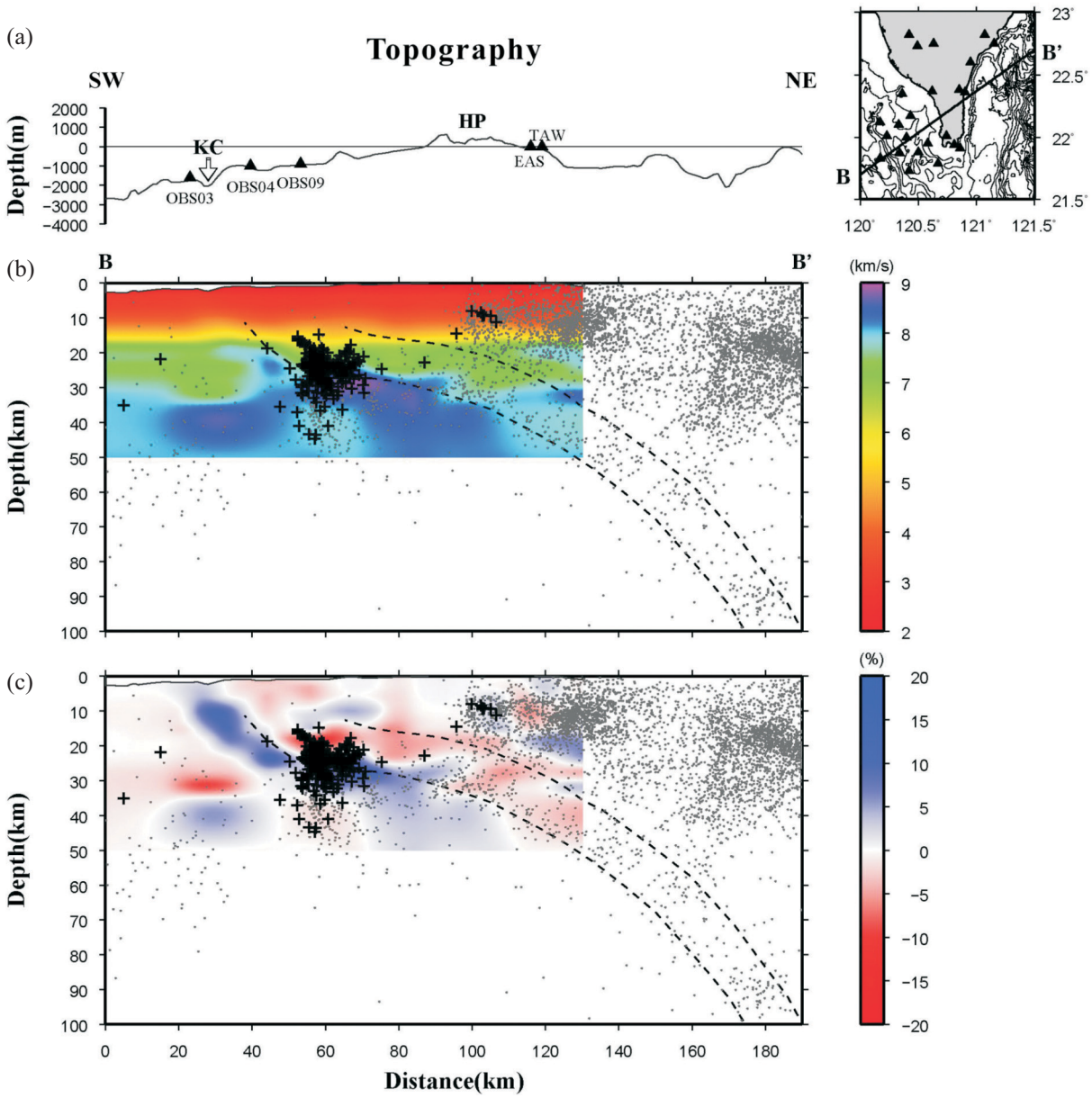

Fig. 11. Earthquake locations along the profile BB'. Dash-lines mark the seismicity zone. The lower dash line indicates the Moho surface. The symbols of black crosses indicate relocated Pingtung earthquake aftershocks while the background earthquakes are plotted in gray dots.

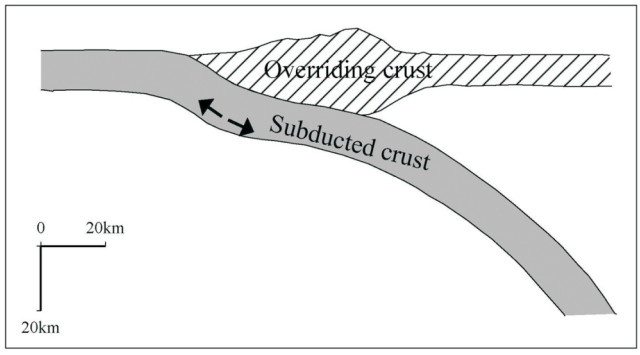

Fig. 12. A schematic model explains an unbending slab off SW Taiwan. The black arrows indicate tensional stress at the lower part of the subducted crust.

REFERENCE

Chen, R. Y., C. W. Ken, W. T. Liang, H. Kao, and R. J. Rau, 2007: Focal mechanism and rupture plane determinations of 2006 Pingtung earthquake sequence. Proceedings, Workshop on Pingtung Earthquakes, Inst. Earth Sci., Academia Sinica, Taipei, Taiwan.

Eberhart-Phillips, D., 1986: Three-dimensional velocity structure in Northern California Coast Ranges from inversion of local earthquake arrival times. *Bull. Seismol. Soc. Am.*, **76**, 1025-1052.

Gardi, A., M. Cocco, A. M. Negredo, R. Sabadini, and S. K. Singh, 2000: Dynamic modeling of the subduction zone of central Mexico. *Geophys. J. Int.*, **143**, 809-820.

Hsu, S. K., 2001: Subduction/collision complexities in the Taiwan-Ryukyu junction area: Tectonics of the Northwestern corner of the Philippine Sea plate. *Terr. Atmos. Ocean. Sci*., **12**, 209-230.

Hsu, S. K., C. S. Liu, C. T. Shyu, S. Y. Liu, J. C. Sibuet, S. Lallemand, C. Wang, and D. Reed, 1998: New gravity and magnetic anomaly maps in the Taiwan-Luzon region and their preliminary interpretation. *Terr. Atmos. Ocean. Sci*., **9**, 509-532.

Hsu, S. K., Y. C. Yeh, W. B. Doo, and C. H. Tsai, 2004: New bathymetry and magnetic lineations identifications in the Northernmost South China Sea and their tectonic implications. *Mar. Geophys. Res*., **25**, 29-44.

Humphreys, E. and R. W. Clayton, 1988: Adaptation of back projection tomography to seismic travel time problems. *J. Geophys. Res*., **93**, 1073-1085.

Kim, K. H., J. M. Chiu, J. Pujol, K. C. Chen, B. S. Huang, Y. H. Yeh, and P. Shen, 2005: Three-dimensional Vp and Vs structural model associated with the active subduction and collision tectonics in the Taiwan region. *Geophys. J. Int*., **162**, 204-220.

Lin, A. T. and A. B. Watts, 2002: Origin of the west Taiwan basin by orogenic loading and flexure of a rifted continental margin. *J. Geophys. Res*., **107**, 2185, doi: 10.1029/2001JB000669.

Lin, J. Y., J. C. Sibuet, C. S. Lee, S. K. Hsu, and F. Klingelhoefer, 2007: Origin of the southern Okinawa Trough volcanism from detailed seismic tomography. *J. Geophys. Res*., **112**, B08308, doi: 10.1029/2006JB004703.

Lo, C. L. and S. K. Hsu, 2005: Earthquake-induced gravitational potential energy change in the active Taiwan orogenic belt. *Geophys. J. Int*., **162**, 169-176.

McIntosh, K., Y. Nakamura, T. K. Wang, R. C. Shih, A. T. Chen, and C. S. Liu, 2005: Crustal-scale seismic profiles across Taiwan and the western Philippine Sea. *Tectonophysics*, **401**, 23-54.

Mikumo, T., Y. Yagi, S. K. Singh, and M. A. Santoyo, 2002: Coseismic and postseismic stress changes in a subducting plate: Possible stress interactions between large interpolate thrust and intraplate normal-faulting earthquakes. *J. Geophys. Res*., **107**, 2023, doi: 10.1029/2001JB000446.

Nakamura, Y., K. McIntosh, and A. T. Chen, 1998: Preliminary results of a large offset seismic survey west of Hengchun Peninsula, southern Taiwan. *Terr. Atmos. Ocean. Sci*., **9**, 395-408.

Seno, T., S. Stein, and A. E. Gripp, 1993: A model for the motion of the Philippine Sea plate consistent with NUVEL-1 and geological data. *J. Geophys. Res*., **98**, 17941-17948.

Sibuet, J. C. and S. K. Hsu, 2004: How was Taiwan created? *Tectonophysics*, **379**, 159-181.

Thurber, C. and D. Eberhart-Phillips, 1999: Local earthquake tomography with flexible gridding. *Comput. Geosci*., **25**, 809-818.

Tsai, C. H., S. K. Hsu, Y. C. Yeh, C. S. Lee, and K. Xia, 2004: Crustal thinning of the northern continental margin of the South China Sea. *Mar. Geophys. Res*., **25**, 63-78.

Wang, C. Y. and T. C. Shin, 1998: Illustrating 100 years of Taiwan seismicity. *Terr. Atmos. Ocean. Sci*., **9**, 589-614.

Wang, Z., D. Zhao, J. Wang, and H. Kao, 2006: Tomographic evidence for the Eurasian lithosphere subducting beneath south Taiwan. *Geophys. Res. Lett*., **33**, L18306, doi: 10.1029/2006GL027166.

Wu, Y. M., C. H. Chang, L. Zhao, J. B. H. Shyu, Y. G. Chen, K. Sieh, and J. P. Avouac, 2007: Seismic tomography of Taiwan: Improved constraints from a dense network of strong-motion stations. *J. Geophys. Res*., **112**, B08312, doi: 10.1029/2007JB004983.

Yeh, Y. C. and S. K. Hsu, 2004: Crustal structures of the Northernmost South China Sea: Seismic reflection and gravity modeling. *Mar. Geophys. Res*., **25**, 45-61.

Yu, H. S. and Y. W. Chou, 2001: Characteristics and development of the flexural forebulge and basal unconformity of western Taiwan foreland basin. *Tectonophysics*, **333**, 277-291.

Yu, S. B., H. Y. Chen, and L. C. Kuo, 1997: Velocity field of GPS stations in the Taiwan area. *Tectonophysics*, **274**, 41-59.

Zhao, D., A. Hasegawa, and S. Horiuchi, 1992: Tomographic imaging of P and S wave velocity structure beneath northeastern Japan. *J. Geophys. Res*., **97**, 19909-19928.